

# OmniSapiens: A Foundation Model for Social Behavior Processing via Heterogeneity-Aware Relative Policy Optimization

Keane Ong<sup>1,2</sup> Sabri Boughorbel<sup>3</sup> Luwei Xiao<sup>1</sup> Chanakya Ekbote<sup>2</sup> Wei Dai<sup>2</sup> Ao Qu<sup>2</sup> Jingyao Wu<sup>2</sup>  
Rui Mao<sup>4</sup> Ehsan Hoque<sup>5</sup> Erik Cambria<sup>4</sup> Gianmarco Mengaldo<sup>†,1</sup> Paul Pu Liang<sup>†,2</sup>

## Abstract

To develop socially intelligent AI, existing approaches typically model human behavioral dimensions (e.g., affective, cognitive, or social attributes) in isolation. Although useful, task-specific modeling often increases training costs and limits generalization across behavioral settings. Recent reasoning RL methods facilitate training a single unified model across multiple behavioral tasks, but do not explicitly address learning across different heterogeneous behavioral data. To address this gap, we introduce HETEROGENEITY-AWARE RELATIVE POLICY OPTIMIZATION (HARPO), an RL method that balances leaning across heterogeneous tasks and samples. This is achieved by modulating advantages to ensure that no single task or sample carries disproportionate influence during policy optimization. Using HARPO, we develop and release OMNISAPIENS-7B 2.0, a foundation model for social behavior processing. Relative to existing behavioral foundation models, OMNISAPIENS-7B 2.0 achieves the strongest performance across behavioral tasks, with gains of up to +16.85% and +9.37% on multitask and held-out settings respectively, while producing more explicit and robust reasoning traces. We also validate HARPO against recent RL methods, where it achieves the most consistently strong performance across behavioral tasks.

## 1. Introduction

One of the longstanding goals in AI is to develop socially-intelligent systems that can perceive, interpret and reason about human behaviors, such as affective expressions, mental states, and social cues (Picard, 2000; Breazeal, 2000).

<sup>†</sup>Equal advising. <sup>1</sup>National University of Singapore <sup>2</sup>MIT  
<sup>3</sup>Qatar Computing Research Institute, HBKU <sup>4</sup>Nanyang Technological University <sup>5</sup>University of Rochester. Correspondence to: Keane Ong <keaneong@mit.edu>. *Preprint*.

However, progress toward this goal has largely proceeded in separate strands, with existing AI models frequently specialized for a single task (i.e., sentiment classification). While useful, task-specific specialization has imposed considerable limitations (Pan et al., 2026). Practically, specialization necessitates bespoke architectures and datasets, leading to an inefficient duplication of modeling effort and computational resources (Gao et al., 2024). More fundamentally, because human behaviors are inherently interconnected (Cambria, 2016), modeling them in isolation overlooks key opportunities for representation sharing across behavioral tasks, reducing generalization and transfer (Ong et al., 2026).

Yet, training unified models across multiple behaviors remains difficult. Behavioral signals are inherently ambiguous and complex, often benefiting from reasoning capabilities (Scherer, 2009). Furthermore, behavioral data is highly heterogeneous, spanning distinct feature types (e.g., acoustic prosody, interpersonal interaction) and prediction targets (e.g., emotion classification (Zadeh et al., 2016), social inference (Wilf et al., 2023)), which can induce uneven learning during multitask training. In this context, while recent RL methods such as GRPO (Shao et al., 2024) support reasoning capabilities in LLMs, they do not explicitly accommodate learning under heterogeneous data. These methods often aggregate policy contributions across tasks and samples without regulating disparities in their learning dynamics, reducing performance by allowing stronger learning signals to disproportionately shape training.

To address these challenges, we develop HETEROGENEITY-AWARE RELATIVE POLICY OPTIMIZATION (HARPO). While supporting reasoning capabilities, HARPO introduces an on-policy advantage modulation mechanism to facilitate balanced learning across heterogeneous behavioral data. Accordingly, HARPO modulates advantages to ensure that no single task or sample disproportionately influences policy optimization. This is achieved by approximating contribution signals to the policy update, and using them to inform geometrically centered and inertially smoothed advantage modulation. Leveraging HARPO, we develop and release OMNISAPIENS-7B 2.0, a foundation model for social behavior processing across 10 behavioral tasks.

Across diverse behavioral tasks on the Human Behavior Atlas benchmark (Ong et al., 2026), OMNISAPIENS-7B 2.0 achieves the strongest performance relative to existing behavioral models, with improvements of up to +16.85% and +9.37% in multitask and held-out settings respectively, while producing more explicit and robust reasoning traces. We additionally compare HARPO against recent critic-free, reasoning RL methods by training on the same benchmark, where it attains the most consistently strong performance across behavioral tasks; improving on GRPO by up to +42.29% on specific tasks.

Our key contribution is two-fold: (1) We develop HARPO, a novel critic-free, reasoning RL method for learning diverse behavioral tasks associated with heterogeneous data; (2) Leveraging HARPO, we train OMNISAPIENS-7B 2.0, a foundation model for unified human behavior analysis that substantially addresses the performance limitations of prior unified models, enabling effective performance across 10 diverse human behavior tasks and generalization to novel behavioral settings. For future work, models and codes will be made publicly available after the review process.

## 2. Related Work

**Social Behavior Processing** aims to develops AI for processing and understanding human behavioral markers. Existing studies have emphasized task-specific modeling, including interpreting *affective states* via emotion classification (Zadeh et al., 2016), arousal–valence prediction (Akçay & Oğuz, 2020; Dang et al., 2023), and affective state ranking (Yannakakis et al., 2018; Wu et al., 2022); *cognitive states* through stress and cognitive load estimation (Giannakakis et al., 2019); *pathological states* by detecting mental health conditions (i.e., depression and anxiety) (Joshi & Kanoongo, 2022; Miloyan et al., 2014); and *social processes* through humor and engagement detection (Hessel et al., 2023; Monkaresi et al., 2016). While useful, task-specific processing overlooks the interdependencies between behavioral dimensions (Pessoa, 2008), motivating unified multi-task approaches to improve generalization through shared representations (Ong et al., 2026).

**Reasoning-Based Reinforcement Learning** has enhanced the reasoning capabilities of LLMs. GRPO (Shao et al., 2024) leverages group-normalized rewards. REINFORCE Leave-One-Out (Ahmadian et al., 2024) reduces gradient variance by computing relative advantages in the same group, while REINFORCE++ (Hu, 2025) improves optimization stability through variance reduction. Group Policy Gradient (Chu et al., 2025) models group-level objectives. In contrast, GRPO-LEAD (Zhang & Zuo, 2025) focuses on shaping reasoning length and difficulty-aware reweighting. Despite these advances, reasoning RL for learning heterogeneous behavioral data remains underexplored.

**Multitask learning** has evolved from unimodal representation sharing (Li et al., 2022; Chen et al., 2025) to any-to-any architectures that jointly model multiple modalities (Bachmann et al., 2024). Beyond architectural advances, prior work has explored multitask optimization via gradient balancing (Yu et al., 2020), uncertainty-based weighting (Kendall et al., 2018), as well as critic-based multitask reinforcement learning via shared distilled policies (Teh et al., 2017) and policy composition (Haarnoja et al., 2018). Yet, multitask learning techniques remain largely underexplored for recent critic-free reasoning reinforcement learning.

## 3. Method

### 3.1. Preliminaries

**Problem Definition: Learning Multiple Behavioral Tasks.** We consider the problem of training a stochastic policy  $\pi_\theta(a | s)$ , instantiated as a large language model (LLM), to perform a diverse set of behavioral understanding tasks indexed by  $m \in \mathcal{M}$ . For each task  $m$ , a sample  $q \sim \mathcal{D}_m$ , which can include multimodal inputs (e.g., text, audio, or visual signals), is drawn from a task-specific input distribution, and the policy generates an autoregressive output sequence  $o \sim \pi_\theta(\cdot | q)$ , with tokens  $o_{:k}$  and prefixes  $o_{:<k}$ . The learning objective is to train a single shared policy  $\pi_\theta$  that maximizes performance across all tasks  $m \in \mathcal{M}$ .

**Group Relative Policy Optimization for Behavioral Tasks.** To optimize  $\pi_\theta(a | s)$ , we consider Group Relative Policy Optimization (GRPO) (Shao et al., 2024), a recent on-policy RL method that has shown strong performance for reasoning-based LLM training. For task  $m$  and sample  $q$ , GRPO samples a rollout group  $G_{(m,q)}$  of responses  $\{o_{(m,q,i)}\}$ , where  $i \in G_{(m,q)}$  indexes individual rollouts (i.e., a sampled response) with rewards  $r_{(m,q,i)}$ , computing the group-normalized advantage:

$$\hat{A}_{(m,q,i)} = \frac{r_{(m,q,i)} - \hat{\mu}_{G_{(m,q)}}}{\hat{\sigma}_{G_{(m,q)}} + \varepsilon}, \quad (1)$$

where  $\hat{\mu}_{G_{(m,q)}}$  and  $\hat{\sigma}_{G_{(m,q)}}$  are the mean and standard deviation of  $\{r_{(m,q,i)}\}_{i=1}^{|G_{(m,q)}|}$ . With a PPO clipped surrogate  $\tilde{A}_{(m,q,i):k}(\theta)$  constructed from  $\hat{A}_{(m,q,i)}$ , GRPO then optimizes  $\pi_\theta(a | s)$  using a PPO-style trust-region objective<sup>1</sup>:

$$J_{\text{GRPO}}(\theta) = \mathbb{E}_{(m,q) \sim \mathcal{D}} \mathbb{E}_{\{o_{(m,q,i)}\} \sim \pi_{\theta_{\text{old}}}} \left[ \frac{1}{|G_{(m,q)}|} \sum_{i \in G_{(m,q)}} \frac{1}{n_{o_{(m,q,i)}}} \sum_{k=1}^{n_{o_{(m,q,i)}}} \tilde{A}_{(m,q,i):k}(\theta) \right] - \beta \mathbb{E}[D_{\text{KL}}(\pi_\theta \| \pi_{\text{ref}})]. \quad (2)$$

<sup>1</sup>For completeness, the full formulation of GRPO is provided in App. D.1.

By the policy-gradient theorem (Sutton et al., 1999), the policy gradient admits the standard form, where the expectation is over  $(s, a)$  induced by  $\pi_\theta$ :

$$\nabla_\theta J(\theta) = \mathbb{E}[A^{\pi_\theta}(s, a) \nabla_\theta \log \pi_\theta(a | s)], \quad (3)$$

When GRPO optimizes a policy across diverse behavioral tasks, gradient contributions from different  $m, q$ , and  $i$  are aggregated into a shared update. Accordingly, a Monte Carlo estimator of the policy gradient,  $g(\theta)$ , can be decomposed as:

$$g(\theta) = \sum_{m \in \mathcal{M}} \sum_{q \sim \mathcal{D}_m} \sum_{i \in G_{(m,q)}} g_{(m,q,i)}(\theta). \quad (4)$$

Each rollout contributes a gradient term of the form:

$$g_{(m,q,i)}(\theta) \triangleq \hat{A}_{(m,q,i)} \nabla_\theta \log \pi_\theta(a_{(m,q,i)} | s_{(m,q,i)}). \quad (5)$$

From Eq.(5), each rollout contributes a gradient term whose magnitude is scaled by its advantage value. Since these rollout-level gradients are aggregated to form the shared policy gradient in Eq.(4), the resulting policy update is sensitive to the scale of advantages across rollouts.

Across diverse behavioral tasks  $m$ , reward and advantage distributions may vary considerably because the associated behavioral data are highly heterogeneous, spanning different multimodal features (e.g., acoustic prosody, facial expressions) and prediction targets (e.g., emotion classification, social inference). Consequently, rollouts from tasks or samples with systematically elevated or suppressed advantage magnitudes can exert disproportionate influence on GRPO’s policy update, contributing to uneven learning across tasks (Sec. 4.5 provides an empirical illustration; App. E.3 Fig. 7 shows the differences in task advantage distributions).

### 3.2. Heterogeneity-Aware Relative Policy Optimization

**Dynamic Advantage Modulation Mechanism.** To address this gap, we introduce HETEROGENEITY-AWARE RELATIVE POLICY OPTIMIZATION (HARPO). Since rollout influence on the policy update scales with advantage magnitude, Eq. (4), HARPO’s core insight is to modulate advantages such that no single task or sample disproportionately influences policy optimization.

In practice, our modulation mechanism scales the GRPO group-normalized advantages, Eq. (1), to mitigate imbalances in advantages at two levels: the sample-level, corresponding to advantages in a sample’s rollout group, and the task-level, corresponding to advantages across all rollout groups of a task. This scaling is updated dynamically across training, using estimates of the relative contribution of each sample and task to the policy update. Concretely, we first

construct a contribution signal  $p^{(t)}$  from advantages, which approximates each task’s and sample’s relative contribution to the shared policy update. These signals are then transformed into structured, geometrically centered modulation factors,  $\{s_{(m,q)}^{(t)}, s_m^{(t)}\}$ , that scale the advantages prior to the policy update step. Finally, the modulation factors are updated using inertial smoothing to ensure their stability.

**Contribution Signals from Advantage Magnitudes.** We construct a proxy signal,  $p^{(t)}$ , to approximate contribution strength to the policy update. Since policy gradients are directly scaled by advantages, Eq.(4)-(5), advantage magnitudes provide a computationally convenient proxy for contribution strength. Therefore, we use advantage magnitudes, normalized by rollout count to ensure invariance to stochastic batch sampling (Schulman et al., 2017), and use this to define  $p^{(t)}$  at two levels. While the sample-level  $p_{(m,q)}^{(t)}$  approximates the contribution of sample  $q$  within a task  $m$ , the task-level  $p_m^{(t)}$  approximates the contribution of a task  $m$ .

Accordingly,  $p_{(m,q)}^{(t)}$  is the average absolute group-normalized advantage over a rollout group  $G_{(m,q)}$  corresponding to a sample  $q$  of a task  $m$  at training step  $t$ .

$$p_{(m,q)}^{(t)} = \frac{1}{|G_{(m,q)}|} \sum_{i \in G_{(m,q)}} |\hat{A}_{(m,q,i)}^{(t)}|. \quad (6)$$

Then, we define  $p_m^{(t)}$  as the average absolute group-normalized advantage over all rollouts collected for task  $m$ , with  $\mathcal{Q}_m^{(t)}$  denoting the set of samples drawn for task  $m$ :

$$p_m^{(t)} = \frac{\sum_{q \in \mathcal{Q}_m^{(t)}} \sum_{i \in G_{(m,q)}} |\hat{A}_{(m,q,i)}^{(t)}|}{\sum_{q \in \mathcal{Q}_m^{(t)}} |G_{(m,q)}|}. \quad (7)$$

**Structured Modulation via a Geometric Reference.** We leverage contribution signals to rebalance influence on the policy update, amplifying samples and tasks with lower contribution signals, and attenuating those with higher ones. Accordingly, we measure how far the contribution signal of each sample and task lay above or below a geometric-mean reference, and proportionately downscale or upscale their associated advantages. On the one hand, taking reference from the geometric-mean ensures that scaling is directly comparable across samples and tasks, and does not change the overall update size. On the other hand, it yields a ratio-based construction of scaling factors that tempers excessive variations in values (as we observe that contribution signals can vary by orders of magnitude, App. E.3 Fig. 6).

Concretely, we define a geometric mean reference at both

the sample-level,  $\bar{p}_{\text{ref},m}^{(t)}$ , and the task-level,  $\bar{p}_{\text{ref},\mathcal{M}}^{(t)}$ :

$$\begin{aligned}\bar{p}_{\text{ref},m}^{(t)} &= \left( \prod_{q \in \mathcal{Q}_m^{(t)}} p_{(m,q)}^{(t)} \right)^{\frac{1}{|\mathcal{Q}_m^{(t)}|}}. \\ \bar{p}_{\text{ref},\mathcal{M}}^{(t)} &= \left( \prod_{m \in \mathcal{M}} p_m^{(t)} \right)^{\frac{1}{|\mathcal{M}|}}\end{aligned}\quad (8)$$

This establishes common baselines for comparing contributions across samples within a task or across tasks overall. For each sample or task contribution signal, we take the reciprocal of its ratio to the geometric-mean. This yields modulation factors  $s_{(m,q)}^{(t)}$  at the sample-level, and  $s_m^{(t)}$  at the task-level.

$$\begin{aligned}s_{(m,q)}^{(t)} &= \frac{\bar{p}_{\text{ref},m}^{(t)}}{p_{(m,q)}^{(t)}}. \\ s_m^{(t)} &= \frac{\bar{p}_{\text{ref},\mathcal{M}}^{(t)}}{p_m^{(t)}}.\end{aligned}\quad (9)$$

The factors scale the group-normalized advantages of each rollout, yielding the HARPO advantage:

$$A_{(m,q,i)}^{(t)} \triangleq s_{(m,q)}^{(t)} s_m^{(t)} \hat{A}_{(m,q,i)}^{(t)}. \quad (10)$$

Due to their reciprocal construction, the modulation factors act to balance advantage magnitudes across samples and tasks. Specifically, within a task, samples whose contribution signals exceed the sample reference (i.e.,  $p_{(m,q)}^{(t)} > \bar{p}_{\text{ref},m}^{(t)}$ ) receive modulation factors  $s_{(m,q)}^{(t)} < 1$ , while those below the reference (i.e.,  $p_{(m,q)}^{(t)} < \bar{p}_{\text{ref},m}^{(t)}$ ) receive  $s_{(m,q)}^{(t)} > 1$ . Consequently, within the same task, stronger samples have downscaled advantages while weaker samples have upscaled advantages. Analogously, at the task-level, the advantages of tasks with contribution signals above the reference  $\bar{p}_{\text{ref},\mathcal{M}}^{(t)}$  are downscaled, while those below the reference are upscaled. Additionally, as the modulation factors are constructed from a geometric mean reference, the factors have a geometric mean of 1. ( $(\prod_{q \in \mathcal{Q}_m^{(t)}} s_{(m,q)}^{(t)}) = 1$  and  $\prod_{m \in \mathcal{M}} s_m^{(t)} = 1$ , App. D.2 shows the full derivation). This ensures that multiplicative upscaling from certain modulation factors are exactly compensated by downscaling from others. Thus, the factors cannot simultaneously enlarge or shrink all advantages at the sample or task-level, mitigating unintended influence on the global step size.

**Inertial control for stable modulation.** We update the modulation mechanism on a slower time scale than the policy parameters. Accordingly, we maintain inertial estimates of both the contribution signals and the modulation factors themselves, allowing modulation to evolve smoothly under stochastic on-policy rollouts. Contribution signals

are smoothed using an exponential moving average to mitigate noise from stochastic rollouts (Kingma & Ba, 2014). Modulation factors, as multiplicative ratios, are smoothed via multiplicative updates rather than by additive adjustments (Arora et al., 2012; Bubeck et al., 2015).

$$\begin{aligned}\bar{p}_{(m,q)}^{(t)} &= \beta_\rho \bar{p}_{(m,q)}^{(t-1)} + (1 - \beta_\rho) p_{(m,q)}^{(t)}. \\ \bar{p}_m^{(t)} &= \beta_\rho \bar{p}_m^{(t-1)} + (1 - \beta_\rho) p_m^{(t)}. \\ s_{(m,q)}^{(t)} &= \left( s_{(m,q)}^{(t-1)} \right)^{\beta_s} (s_{(m,q)})^{1-\beta_s}. \\ s_m^{(t)} &= \left( s_m^{(t-1)} \right)^{\beta_s} (s_m)^{1-\beta_s}.\end{aligned}\quad (11)$$

This inertial smoothing ensures that the modulation factors respond to persistent trends in contribution signals, rather than to stochastic on-policy fluctuations in their values.

**HARPO<sup>2</sup> Objective.** With the HARPO-modulated advantage in place, HARPO retains the PPO-style trust-region objective of GRPO, substituting  $A^H$  for  $\hat{A}$  to construct the clipped surrogate  $\tilde{A}_{(m,q,i):k}^H(\theta)$ , thereby forming the HARPO objective:

$$\begin{aligned}J_{\text{HARPO}}(\theta) &= \mathbb{E}_{(m,q) \sim \mathcal{D}} \mathbb{E}_{\{o_{(m,q,i)}\} \sim \pi_{\theta_{\text{old}}}} \left[ \frac{1}{|G_{(m,q)}|} \sum_{i \in G_{(m,q)}} \right. \\ &\quad \left. \frac{1}{n_{o_{(m,q,i)}}} \sum_{k=1}^{n_{o_{(m,q,i)}}} \tilde{A}_{(m,q,i):k}^H(\theta) \right] - \beta \mathbb{E}[D_{\text{KL}}(\pi_\theta \parallel \pi_{\text{ref}})].\end{aligned}\quad (12)$$

### 3.3. Reward Design

**Accuracy.** For classification tasks, we use a binary reward  $r_{\text{cls}}$ , which equals 1 for an exact label match and 0 otherwise. For question-answering tasks with free-text responses, we use cosine similarity rewards,  $r_{qa}$ , normalized to a scale of  $[0, 1]$  for compatibility with rewards assignment, to measure alignment between the generated response and answer.

**Formatting.** We add a binary reward,  $r_{\text{fmt}}$ , for adhering to the response structure, which includes reasoning traces followed by the model’s prediction.

**Length.** Following Zhang & Zuo (2025), we leverage an overlong length penalty,  $r_{\text{len}}$ , to prevent excessive verbosity of responses.

**Final reward<sup>2</sup>.** With format weight  $w_{\text{fmt}} = 0.2$  and length scale  $\lambda_{\text{len}} = 0.75$ , the final per-sample reward is the following, where  $r_{\text{task}}$  can be  $r_{\text{cls}}$  or  $r_{qa}$ , depending on if the sample belongs to a classification or QA task respectively.

$$r = (1 - w_{\text{fmt}}) r_{\text{task}} + w_{\text{fmt}} r_{\text{fmt}} + \lambda_{\text{len}} r_{\text{len}},$$

<sup>2</sup>App. A Algorithm 1 summarizes HARPO. Additional details of reward design are in App. C.2

Table 1. Per-task performance (%) is reported for both models and training algorithms. Each task may include multiple datasets; we report the mean performance across a task’s associated datasets, with full results in App. Tab. 7. Following Ong et al. (2026), we report binary weighted F1 for SEN; mean per-class weighted accuracy for EMO; weighted F1 for HUM, SAR, ANX, DEP, and PTSD; and LLM-Judge accuracy for SOC, INT, and NVC. Given the disparities between the metrics, we compute average performance rank across tasks separately for models and algorithms ( $\downarrow$  indicates lower score is better), with ties assigned the same rank. Best results are bolded and second-best are underlined. (\*) denotes existing models that have been trained on more than two behavioral tasks, reflecting substantive multitask training; only a few such models are publicly available. For fair comparison, all training algorithm results reflect training on the same Human Behavior Atlas benchmark, using an identical reward design (Sec. 3.3) and the same base model (Qwen2.5-Omni-7B).

Models	EMO	HUM	INT	PTSD	ANX	DEP	SEN	SAR	SOC	NVC	Avg. Rank $\downarrow$
Gemma-3-4B (Team et al., 2025)	55.03	59.70	22.70	49.90	60.10	46.25	73.83	52.90	19.10	2.30	5.90
Qwen 2.5-Omni-7B (Xu et al., 2025a)	58.25	54.30	25.40	76.00	79.30	71.35	67.20	<u>65.60</u>	25.40	6.90	4.20
Qwen 2.5-VL-7B (Bai et al., 2025)	54.08	58.30	24.90	75.50	63.10	63.80	50.50	<u>51.10</u>	23.10	9.80	5.60
Qwen 3-VL-8B-Instruct (Xu et al., 2025b)	57.66	66.76	38.00	92.70	42.29	51.62	69.70	63.67	24.94	<u>13.95</u>	4.00
OmniSapiens-7B RL* (Ong et al., 2026)	57.28	<u>63.90</u>	48.60	96.80	91.90	<u>77.15</u>	39.60	64.70	<b>30.40</b>	<u>13.30</u>	3.00
HumanOmniV2-7B* (Yang et al., 2025)	<u>59.70</u>	63.80	26.30	82.40	52.70	65.40	74.20	39.50	<u>28.20</u>	9.30	4.00
<b>OmniSapiens-7B 2.0 (ours)</b>	<b>76.55</b>	<b>69.85</b>	<b>50.52</b>	<b>98.39</b>	<b>91.98</b>	<b>78.87</b>	<b>77.61</b>	<b>70.64</b>	25.40	<b>14.54</b>	<b>1.20</b>
<b>Training Algorithms</b>											
RLOO (Ahmadian et al., 2024)	75.58	67.86	<u>51.73</u>	<b>98.39</b>	90.68	77.57	76.86	<u>62.58</u>	<b>29.54</b>	<b>16.28</b>	2.50
RE++ (Hu, 2025)	75.92	60.26	<u>5.01</u>	<b>98.39</b>	<b>93.11</b>	73.87	56.52	<u>50.21</u>	12.64	4.07	3.90
GPG (Chu et al., 2025)	<b>77.70</b>	<u>69.28</u>	<b>54.21</b>	<b>98.39</b>	90.40	<u>78.40</u>	75.77	45.96	<u>27.93</u>	12.79	2.50
GRPO (Shao et al., 2024)	76.45	27.56	49.90	<b>98.39</b>	90.40	<u>77.64</u>	<u>77.51</u>	53.58	23.30	11.00	3.30
<b>HARPO (ours)</b>	<u>76.55</u>	<b>69.85</b>	50.52	<b>98.39</b>	<u>91.98</u>	<b>78.87</b>	<b>77.61</b>	<b>70.64</b>	25.40	<u>14.54</u>	<b>1.70</b>

## 4. Experiments

### 4.1. Setup

We use the Human Behavior Atlas benchmark (Ong et al., 2026) for training and evaluation, which covers diverse human behavior tasks with over 100k samples. The tasks include sentiment polarity (SEN), emotion recognition (EMO), social reasoning (SOC), intent recognition (INT), non-verbal communication (NVC), as well as detecting humor (HUM), sarcasm (SAR), anxiety (ANX), depression (DEP), and PTSD (PTSD). Given the multimodal nature of the data (text, vision, and audio), we adopt Qwen 2.5 Omni-7B (Xu et al., 2025a) as our base architecture for OMNISAPIENS-7B 2.0. All training follows a multitask setup, where a single model is jointly trained across all tasks.

### 4.2. Multitask Performance

RQ1: We compare HARPO with recent critic-free reasoning RL methods by training all methods on the same benchmark with an identical reward design and base model (Qwen 2.5 Omni-7B). We also evaluate our HARPO-trained model, OMNISAPIENS-7B 2.0, against state-of-the-art models.

**Comparing Model Performance.** Relative to existing models, OMNISAPIENS-7B 2.0 achieves the strongest overall performance across behavioral tasks. From Tab. 1, OMNISAPIENS-7B 2.0 outperforms general-purpose LLMs (Gemma-3, Qwen-2.5-Omni, Qwen-2.5-VL, Qwen-3-VL). It also outperforms prior behavioral models trained jointly on multiple diverse social-behavioral tasks, for which only a small number of public models exist (HumanOmniV2-7B, OmniSapiens-7B RL). In particular, OMNISAPIENS-7B 2.0 achieves the best results on 9 of 10 tasks and attains the strongest average task performance rank (1.20).

**RL Algorithm Performance Comparison.** HARPO exhibits the most consistent performance across behavioral tasks among recent reasoning RL algorithms. From Tab. 1, HARPO outperforms widely adopted reasoning-based RL methods that follow critic-free training paradigms (e.g., GRPO, RLOO) and their subsequent variants (GPG, RE++), achieving the best average performance rank (1.70) across tasks. Notably, while GRPO, GPG, RE++ exhibit performance collapse on certain tasks (i.e., SAR) the weaker-performing tasks under HARPO do not experience such collapse, suggesting relatively balanced multitask learning.

### 4.3. Generalization Performance

Table 2. Zero-shot generalization weighted F1 performance (%) on AUT and SER, compared to existing models.

Model	AUT	SER
Qwen 2.5-Omni-7B	25.68	53.53
OmniSapiens-7B RL	30.46	55.77
HumanOmniV2-7B	<u>38.05</u>	<u>62.74</u>
<b>OmniSapiens-7B 2.0 (ours)</b>	<b>39.91</b>	<b>72.11</b>

RQ2: We analyze zero-shot transfer performance on held-out datasets (i.e., without further fine-tuning) to evaluate the generalization capabilities of OMNISAPIENS-7B 2.0 relative to existing behavioral models. Specifically, we evaluate on AV-ASD (Deng et al., 2024) for the task of Autism Behavior Recognition (AUT) and on IEMOCAP (Busso et al., 2008) for Speech Emotion Recognition (SER).

**Transfer Performance on AUT.** AUT focuses on recognizing autism-related behavioral cues, a data-scarce domain where high annotation costs and privacy constraints limit

data availability for supervised training (Li et al., 2023a). OMNISAPIENS-7B 2.0 attains the highest performance of 39.91%, outperforming HumanOmniV2-7B (38.05%) and OmniSapiens-7B RL (30.46%) by approximately +2% and +9%, respectively. This suggests how OMNISAPIENS-7B 2.0 can be more effective in data-scarce behavioral settings such as autism without explicit supervision, by enabling stronger transfer from general behavioral training.

**Transfer Performance on SER.** OMNISAPIENS-7B 2.0 achieves the highest zero-shot performance on SER, which suggests greater generalization performance for emotion recognition. Although SER is related to emotion recognition (EMO), it is evaluated on a held-out dataset (IEMOCAP) that differs substantially from the benchmark’s EMO training datasets in annotation protocols and conversational context. These annotation and contextual differences often pose challenges for model generalization in emotion recognition settings (Montag et al., 2025). Yet, OMNISAPIENS-7B 2.0 reaches 72.11%, exceeding HumanOmniV2-7B (62.74%) and OmniSapiens-7B RL (55.77%) by roughly +9% and +16%, respectively. This suggests that OMNISAPIENS-7B 2.0 can support more robust transfer to new emotion recognition settings.

**Comparison with OmniSapiens-7B RL.** Despite being trained on the same Human Behavioral Atlas benchmark, OMNISAPIENS-7B 2.0, trained with HARPO, exhibits stronger generalization performance than OmniSapiens-7B RL on SER and AUT. This coincides with the more balanced multitask performance achieved by OMNISAPIENS-7B 2.0 from Tab. 1, with an average task rank of 1.20 compared to 3.00 for OmniSapiens-7B RL. This suggests that the HARPO-trained OMNISAPIENS-7B 2.0, by learning more uniformly across behavioral tasks, can support the acquisition of general behavioral features that are more transferable, contributing to improved generalization performance.

#### 4.4. Reasoning Comparison

RQ3: Beyond task performance, we compare reasoning traces<sup>3</sup> for an interpretable view of the decision-making process of different methods and models. This provides insight into the robustness of the underlying inference behavior.

**Reasoning on Complex Pragmatic Tasks.** For complex tasks such as sarcasm (SAR) and humour (HUM) detection, which rely on pragmatic cues (i.e., contextual signals beyond literal lexical content), we observe that HARPO induces richer reasoning behavior as compared to GRPO. From Fig. 1, compared to GRPO, HARPO achieves a larger proportion of correct predictions on SAR and HUM, accompanied by longer and more varied reasoning-length dis-

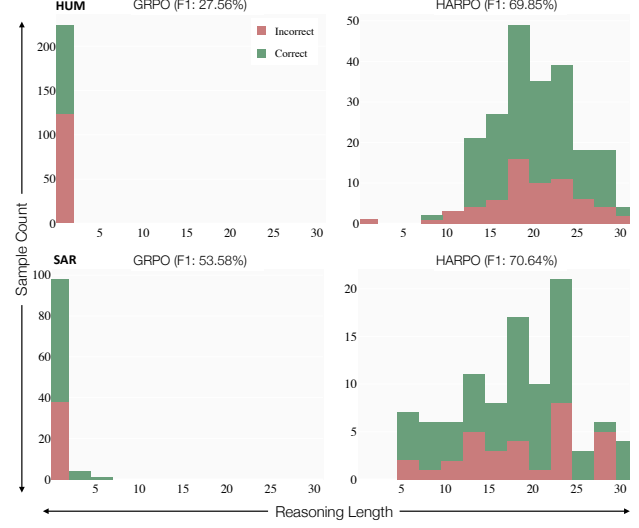


Figure 1. Sample count versus token reasoning length. Green indicates correct predictions, red indicates incorrect. HARPO induces more varied reasoning lengths for the respective tasks of (Top: HUM, Bottom: SAR), compared to GRPO.

 <p>Transcript: "That's why I began investigating the most secretive and experimental prison units in the United States for so-called second-tier terrorists"</p> <p>Q: Does this video contain a humorous punchline?</p>	 <p>Transcript: "I can't believe we wasted all that time on our Hulk costumes."</p> <p>Q: Is the speaker being sarcastic in this utterance?</p>
<p><b>HARPO:</b></p> <p>Reasoning: The speaker is talking about a serious topic, investigating prison units, which is not a humorous punchline.</p> <p>Classification: Not Humour ✓</p> <p><b>GRPO:</b></p> <p>Reasoning: Humour</p> <p>Classification: Humour ✗</p>	<p><b>HARPO:</b></p> <p>Reasoning: The speaker is expressing disappointment and frustration about wasting time on Hulk costumes, which is not a sarcastic comment.</p> <p>Classification: Not Sarcasm ✓</p> <p><b>GRPO:</b></p> <p>Reasoning: Sarcasm</p> <p>Classification: Sarcasm ✗</p>

Figure 2. Example of reasoning traces on pragmatic tasks humour detection (HUM) (left) and sarcasm detection (SAR) (right). HARPO is observed to reflect more explicit and varied reasoning compared to GRPO, which defaults to minimal/ no reasoning.

tributions. Qualitative analysis, Fig. 2, further illustrates that GRPO often produces shortcut responses with minimal or no explicit reasoning, while HARPO’s reasoning traces remain more contextually grounded, reflecting deliberation over pragmatic and inferential cues present in the input. These findings suggest that HARPO’s emphasis on balanced optimization reduces the suppression of useful reasoning trajectories for these weaker tasks, resulting in richer reasoning behavior that coincides with improved task performance.

**Reasoning in Zero-Shot Settings.** On the held-out AUT task, qualitative analysis of reasoning traces, Fig. 3, reveals that HumanOmniV2 often generates expansive reasoning chains that can introduce additional behaviors without clear evidential support. This tendency is reflected by a higher average number of predicted behaviors per sample (2.38) than are present (1.72). Conversely, OmniSapiens-7B RL often reasons that autism behaviors are absent even when salient

<sup>3</sup>To support reproducibility and further study, we make publicly available all the reasoning traces after the review process.

 <p>Q: Based on the audio and video, which of the autism-related behaviors are present? (Definitions of behaviors are provided, i.e.: Aggressive Behavior: ... Non-Responsiveness: ... ...)</p> <p>You may respond with one or more behavior.</p>	<b>HumanOmniv2:</b> Reasoning: He's standing and just swinging his arms really fast and hard. That could definitely be seen as aggressive behavior... He's moving so fast too, looking quite agitated. This could be linked to hyperactivity, which might be part of sensory overresponsive behavior... He's sitting at the table, hands covering his face, looking distressed... maybe non-responsive to what's happening around him...	<b>OmniSapiens RL:</b> Reasoning: The audio and video do not provide enough information to determine the presence of the autism-related behaviors listed. The background (label) is indicated as "no significant target behavior present"	<b>OmniSapiens 2.0:</b> Reasoning: The children are hitting each other, which is aggressive behavior
	<b>Classification:</b> Aggressive Behavior: Hyper- or Hyporeactivity to Sensory Input, Non-Responsiveness to Verbal Interaction <span style="color: red;">✗</span>	<b>Classification:</b> Background <span style="color: red;">✗</span>	<b>Classification:</b> Aggressive Behavior <span style="color: green;">✓</span>

Figure 3. Reasoning traces on zero-shot generalization for autism behavioral detection (AUT) on the AVASD dataset; HumanOmniv2 tends to produce verbose reasoning, OmniSapiens RL tends to abstain from making predictions, OMNISAPIENS-7B 2.0 generates concise reasoning traces identifying the most salient behavior.

cues are visible; it predicts “background (no behavior)” in 44.76% of samples, although such cases only account for 4.20%. In contrast, the HARPO-trained OMNISAPIENS-7B 2.0 typically produces concise reasoning traces that focus on identifying salient behaviors directly supported by the clip’s evidence, without overpredicting (1.07 predictions per sample) or defaulting to “background (no behavior)” predictions (only 18.31% of such predictions across samples). While this stricter, evidence-based reasoning style yields lower recall than HumanOmniV2 (32.38% versus 46.75%), it substantially improves precision (51.97% versus 33.72%), and avoids the conservative abstention behavior observed in OmniSapiens-7B RL, leading to the strongest overall performance (F1 of 39.91 in Tab. 2) among the compared models. These observations on AUT indicate that relative to existing models, OMNISAPIENS-7B 2.0’s evidence-aligned reasoning behavior yields a more effective precision–recall trade-off by mitigating over-prediction and abstention, suggesting its potential utility for zero-shot behavioral detection.

#### 4.5. Empirical Analysis & Ablations

RQ4: To further evaluate the mechanisms of HARPO, we conduct empirical analyses and ablation studies to examine the behavior of its underlying mechanisms.

**Effect of HARPO’s Advantage Modulation on Weak Performing Tasks.** A central design principle of HARPO is to promote balanced optimization by modulating advantages prior to the policy update step. To investigate this effect, we compute the relative task advantage, defined as the ratio between a task’s average advantage magnitude and the mean of the average advantage magnitudes across all tasks, to observe how a change in this statistic affects learning. We focus on the SAR task as a representative weak-performing

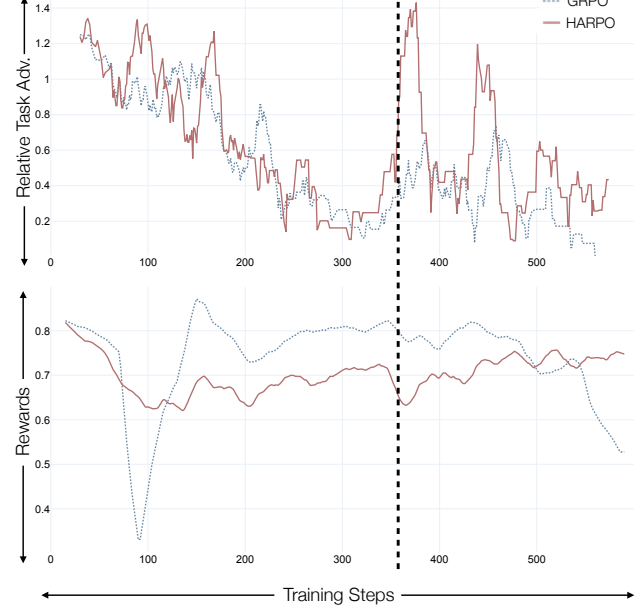


Figure 4. Comparison of relative task advantage and rewards for SAR under HARPO and GRPO. After step 355 (dotted line), HARPO exhibits increasing relative task advantage alongside increasing rewards, while GRPO maintains lower relative task advantage with decreasing rewards.

task (performance of 53.58% under GRPO; 70.64% under HARPO), which allows us to more clearly study advantage modulation in this regime. We track how its relative task advantage evolves over 600 training steps, alongside task rewards. From Fig. 4, in the later parts of training (i.e., after the dotted line depicting step 355), HARPO’s amplification of SAR’s relative task advantage coincides with a continued increase in average rewards. At the same late-stage of training, GRPO’s unmodulated relative task advantage remains lower, corresponding with a steady decline in rewards. This suggests that HARPO’s advantage modulation can help sustain longer learning for weak-performing tasks with otherwise diminished advantages, contributing to improved task performance.

Table 3. Average task performance rank for HARPO ablations (lower is better), computed by ranking methods per task based on performance, then averaging ranks across tasks. We provide the per-task and per-dataset performance breakdown in App. E.1.

Variant	Avg. Rank $\downarrow$
HARPO	1.90
w/o structured modulation	2.00
w/o sample-level modulation	2.60
w/o inertial control	2.70

**Effect of Structured Modulation.** We consider an ablation in which structured modulation via the geometric reference is removed, and advantage modulation factors are instead the inverse of the contribution signals (i.e.,  $s^{(t)} = 1/p^{(t)}$ ). From Tab. 3, this variant (w/o structured modulation) ex-

hibits weaker multitask performance (avg. rank 2.00) compared to HARPO (1.90). A possible explanation is that the ablation produces a net amplification of advantages during training. The per-task modulation factors  $s_m^{(t)}$  have a geometric mean that remains above atleast 2.5 (App. Fig. 6), indicating a sustained tendency for advantages to be upscaled during training. In contrast, due to geometric centering, HARPO maintains a modulation factors that have a geometric mean of 1, mitigating uniform amplification of advantages across tasks. Since the magnitude of policy-gradient updates is directly scaled by advantage values, increasing advantage magnitudes can alter the effective update size, which is known to influence optimization behavior and performance (Schulman et al., 2015; 2017). As a result, directly using  $s^{(t)} = 1/p^{(t)}$  instead of a structured, geometrically centered modulation may inadvertently impact optimization dynamics and downstream performance.

**Effect of Inertial Control.** From Tab. 3, the average rank degrades from 1.90 with the HARPO method to 2.70 for the ablation without inertial control (i.e. without smoothing in Eq. 11). To study this further, we examine the task modulation factors  $s_m^{(t)}$  over training for multiple tasks (SAR, SEN, ANX). From Fig. 5, we observe that tasks with greater performance improvements with inertial control, SAR (+7.96%) and SEN (+5.69%) from App. E Tab. 5, also exhibit clearer differences in  $s_m^{(t)}$  over training. In particular, inertial control yields more gradual changes in  $s_m^{(t)}$ , in contrast to the sharper fluctuations observed without it. In contrast, ANX, which exhibits comparatively smaller performance differences (+1.30%), shows similar  $s_m^{(t)}$  trends with and without inertial control. This suggest that while inertial control does not uniformly affect all tasks, it can improve performance for tasks with excessive fluctuations in  $s_m^{(t)}$ , by stabilizing the scaling of advantage signals, which can support more consistent policy updates (Ilyas et al., 2018).

**Effect of Modulation at the Sample-Level.** To study the effect of modulating advantages at the sample-level in addition to the task-level, we run an ablation without sample-level modulation (i.e. leveraging only the task-level modulation factors,  $s_m^{(t)}$ ). From Tab. 3, this results in weaker overall performance, with the ablation attaining a 2.60 average task performance rank compared to HARPO at 1.90. To understand the impact of sample-level modulation, we analyze with Fig. 5, a task (ANX) that performs stronger with modulation at the sample-level. Accordingly, we observe that modulation at the sample-level produces a noticeably narrower advantage distribution compared to without, highlighting that relatively extreme advantage values are suppressed (we observe the same trend for other tasks as well, with more plots provided for NVC, SOC, HUM in App. E.3 Fig. 7). This narrower spread does not necessarily indicate a reduction in the aggregate advantages, since the geometric

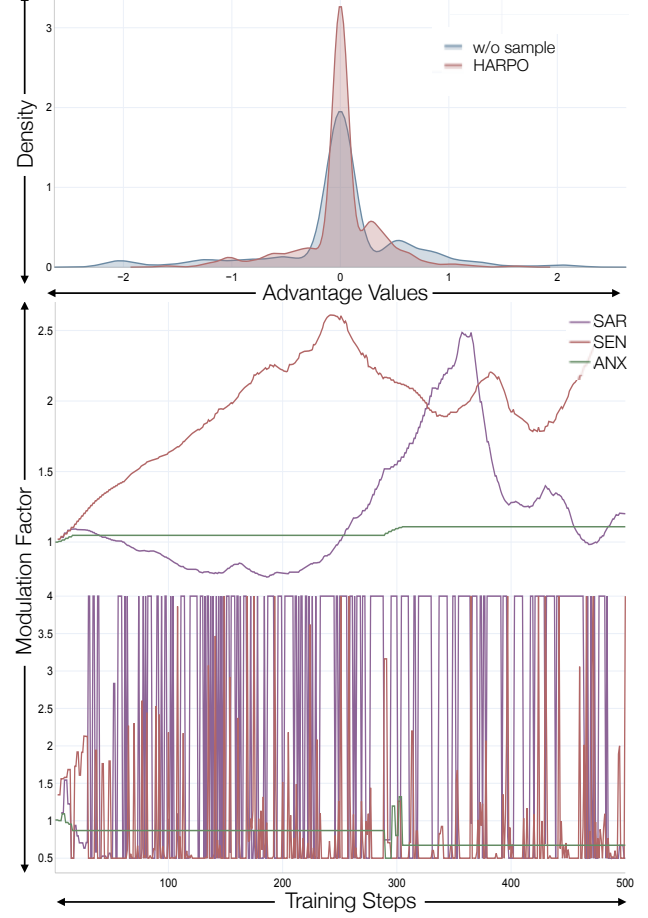


*Figure 5.* Top: Comparison of distribution of advantages between HARPO and the ablation without sample-level modulation, for the ANX task. Sample-level modulation leads to a narrowing of the advantage distribution which can result in better performance for specific tasks (additional task distributions are in App. E). Middle & Bottom: Comparison of modulation factors between HARPO (middle) and without inertial control (bottom). Inertial control enables a more gradual change in modulation factor values.

mean enforced by Eqs. (8)-(9) helps preserve the overall multiplicative scale of scaled advantages. Instead, it mitigates extreme advantage values; potentially preventing a small subset of samples with extreme values from disproportionately influencing the policy update. However, while beneficial for most tasks, the effects of sample-level modulation varies across tasks, as EMO, INT, and SOC show no explicit improvements (App. E.1 Fig. 5).

## 5. Conclusion

In this work, we introduced HARPO, a RL method that accounts for heterogeneous learning signals across multiple behavioral tasks. Using HARPO, we developed OmniSapiens 2.0, a unified behavioral model trained on diverse datasets. Multitask and generalization evaluations showed consistent

performance across behavioral domains, underscoring the value of modeling heterogeneous learning signals.

More broadly, these findings suggest a different perspective in how unified social behavioral AI may be trained. Rather than assuming that the strongest signals are inherently the most informative, unified models may benefit from explicitly protecting weaker, but structurally meaningful signals that encode latent social and behavioral structure.

## Impact Statement

This paper presents work whose goal is to advance the field of Machine Learning. There are many potential societal consequences of our work, none which we feel must be specifically highlighted here.

## References

Ahmadian, A., Cremer, C., Gallé, M., Fadaee, M., Kreutzer, J., Pietquin, O., Üstün, A., and Hooker, S. Back to basics: Revisiting reinforce style optimization for learning from human feedback in llms. *arXiv preprint arXiv:2402.14740*, 2024.

Akçay, M. B. and Oğuz, K. Speech emotion recognition: Emotional models, databases, features, preprocessing methods, supporting modalities, and classifiers. *Speech Communication*, 116:56–76, 2020.

Arora, S., Hazan, E., and Kale, S. The multiplicative weights update method: a meta-algorithm and applications. *Theory of computing*, 8(1):121–164, 2012.

Bachmann, R., Kar, O. F., Mizrahi, D., Garjani, A., Gao, M., Griffiths, D., Hu, J., Dehghan, A., and Zamir, A. 4m-21: An any-to-any vision model for tens of tasks and modalities. *Advances in Neural Information Processing Systems*, 37:61872–61911, 2024.

Bai, S., Chen, K., Liu, X., Wang, J., Ge, W., Song, S., Dang, K., Wang, P., Wang, S., Tang, J., et al. Qwen2. 5-vl technical report. *arXiv preprint arXiv:2502.13923*, 2025.

Breazeal, C. L. *Sociable machines: Expressive social exchange between humans and robots*. PhD thesis, Massachusetts Institute of Technology, 2000.

Bubeck, S. et al. Convex optimization: Algorithms and complexity. *Foundations and Trends® in Machine Learning*, 8(3-4):231–357, 2015.

Busso, C., Bulut, M., Lee, C.-C., Kazemzadeh, A., Mower, E., Kim, S., Chang, J., Lee, S., and Narayanan, S. S. Iemocap: Interactive emotional dyadic motion capture database. *Journal of Language Resources and Evaluation*, 42(4):335–359, dec 2008. doi: 10.1007/s10579-008-9076-6.

Cambria, E. Affective computing and sentiment analysis. *IEEE Intelligent Systems*, 31(2):102–107, 2016.

Cao, H., Cooper, D. G., Keutmann, M. K., Gur, R. C., Nenkova, A., and Verma, R. Crema-d: Crowd-sourced emotional multimodal actors dataset. *IEEE transactions on affective computing*, 5(4):377–390, 2014.

Castro, S., Hazarika, D., Pérez-Rosas, V., Zimmermann, R., Mihalcea, R., and Poria, S. Towards multimodal sarcasm detection (an \_obviously\_ perfect paper). In *ACL*, 2019.

Chen, J., Yang, J., Wu, H., Li, D., Gao, J., Zhou, T., and Xiao, B. Florence-vl: Enhancing vision-language models with generative vision encoder and depth-breadth fusion. In *Proceedings of the Computer Vision and Pattern Recognition Conference*, pp. 24928–24938, 2025.

Chu, X., Huang, H., Zhang, X., Wei, F., and Wang, Y. Gpg: A simple and strong reinforcement learning baseline for model reasoning. *arXiv preprint arXiv:2504.02546*, 2025.

Dang, T., Dimitriadis, A., Wu, J., Sethu, V., and Ambikairajah, E. Constrained dynamical neural ode for time series modelling: A case study on continuous emotion prediction. In *ICASSP 2023-2023 IEEE International Conference on Acoustics, Speech and Signal Processing (ICASSP)*, pp. 1–5. IEEE, 2023.

Deng, S., Kosloski, E. E., Patel, S., Barnett, Z. A., Nan, Y., Kaplan, A., Aarukapalli, S., Doan, W. T., Wang, M., Singh, H., et al. Hear me, see me, understand me: Audio-visual autism behavior recognition. *IEEE Transactions on Multimedia*, 2024.

Gao, S., Koker, T., Queen, O., Hartvigsen, T., Tsiligkaridis, T., and Zitnik, M. Units: A unified multi-task time series model. *Advances in Neural Information Processing Systems*, 37:140589–140631, 2024.

Giannakakis, G., Grigoriadis, D., Giannakaki, K., Simantiraki, O., Roniotis, A., and Tsiknakis, M. Review on psychological stress detection using biosignals. *IEEE transactions on affective computing*, 13(1):440–460, 2019.

Haarnoja, T., Pong, V., Zhou, A., Dalal, M., Abbeel, P., and Levine, S. Composable deep reinforcement learning for robotic manipulation. In *2018 IEEE international conference on robotics and automation (ICRA)*, pp. 6244–6251. IEEE, 2018.

Hasan, M. K., Rahman, W., Zadeh, A. B., and Zhong, J. Ur-funny: A multimodal language dataset for understanding humor. In *EMNLP-IJCNLP*, pp. 2046–2056, 2019.

Henderson, P., Islam, R., Bachman, P., Pineau, J., Precup, D., and Meger, D. Deep reinforcement learning that matters. In *Proceedings of the AAAI conference on artificial intelligence*, volume 32, 2018.

Hessel, J., Marasović, A., Hwang, J. D., Lee, L., Da, J., Zellers, R., Mankoff, R., and Choi, Y. Do androids laugh at electric sheep? humor “understanding” benchmarks from the new yorker caption contest. In *Proceedings of the 61st Annual Meeting of the Association for Computational Linguistics (Volume 1: Long Papers)*, pp. 688–714, 2023.

Hu, J. Reinforce++: A simple and efficient approach for aligning large language models. *arXiv preprint arXiv:2501.03262*, 2025.

Ilyas, A., Engstrom, L., Santurkar, S., Tsipras, D., Janoos, F., Rudolph, L., and Madry, A. A closer look at deep policy gradients. *arXiv preprint arXiv:1811.02553*, 2018.

Joshi, M. L. and Kanoongo, N. Depression detection using emotional artificial intelligence and machine learning: A closer review. *Materials Today: Proceedings*, 58:217–226, 2022.

Kendall, A., Gal, Y., and Cipolla, R. Multi-task learning using uncertainty to weigh losses for scene geometry and semantics. In *Proceedings of the IEEE Conference on Computer Vision and Pattern Recognition*, pp. 7482–7491, 2018.

Kingma, D. and Ba, J. Adam: A method for stochastic optimization. *arXiv preprint arXiv:1412.6980*, 2014.

Li, H., Tjandrasuwita, M., Fung, Y. R., Solar-Lezama, A., and Liang, P. P. Mimeqa: Towards socially-intelligent nonverbal foundation models. *arXiv preprint arXiv:2502.16671*, 2025.

Li, J., Li, D., Xiong, C., and Hoi, S. Blip: Bootstrapping language-image pre-training for unified vision-language understanding and generation. In *International Conference on Machine Learning*, pp. 12888–12900. PMLR, 2022.

Li, J., Chheang, V., Kullu, P., Brignac, E., Guo, Z., Bhat, A., Barner, K. E., and Barmaki, R. L. Mmasd: A multimodal dataset for autism intervention analysis. In *Proceedings of the 25th International Conference on Multimodal Interaction*, pp. 397–405, 2023a.

Li, J., Wei, P., Han, W., and Fan, L. Intentqa: Context-aware video intent reasoning. In *Proceedings of the IEEE/CVF international conference on computer vision*, pp. 11963–11974, 2023b.

Liang, P. P., Salakhutdinov, R., and Morency, L.-P. Computational modeling of human multimodal language: The mosei dataset and interpretable dynamic fusion. In *ACL*, 2018.

Miloyan, B., Pachana, N. A., and Suddendorf, T. The future is here: A review of foresight systems in anxiety and depression. *Cognition & emotion*, 28(5):795–810, 2014.

Monkaresi, H., Bosch, N., Calvo, R. A., and D’Mello, S. K. Automated detection of engagement using video-based estimation of facial expressions and heart rate. *IEEE Transactions on Affective Computing*, 8(1):15–28, 2016.

Montag, C., Xu, C., Spapé, M., and Cambria, E. The emotion labeling problem in affective computing research. 2025.

Ong, K., Dai, W., Li, C., Feng, D., Li, H., Wu, J., Cheong, J., Mao, R., Mengaldo, G., Cambria, E., et al. Human behavior atlas: Benchmarking unified psychological and social behavior understanding. In *Proceedings of ICLR*, 2026.

OpenAI. Gpt-5. <https://openai.com/gpt-5/>, August 2025.

Pan, R., Luo, H., Yuan, Q., Luo, G., Li, J., Shen, T., Mao, R., and Cambria, E. Multitask reinforcement learning with metadata-guided adaptive routing. *Information Fusion*, 129:104068, 2026.

Pessoa, L. On the relationship between emotion and cognition. *Nature reviews neuroscience*, 9(2):148–158, 2008.

Picard, R. W. *Affective computing*. MIT press, 2000.

Pichora-Fuller, M. K. and Dupuis, K. Toronto emotional speech set (TESS). *Borealis*, 2020. doi: 10.5683/SP2/E8H2MF. URL <https://doi.org/10.5683/SP2/E8H2MF>.

Poria, S., Hazarika, D., Majumder, N., Naik, G., Cambria, E., and Mihalcea, R. MELD: A multimodal multi-party dataset for emotion recognition in conversations. In *ACL*, pp. 527–536, 2019.

Sawadogo, M. A. L., Pala, F., Singh, G., Selmi, I., Puteaux, P., and Othmani, A. Ptsd in the wild: a video database for studying post-traumatic stress disorder recognition in unconstrained environments. *Multimedia Tools and Applications*, 83(14):42861–42883, 2024.

Scherer, K. R. The dynamic architecture of emotion: Evidence for the component process model. *Cognition and emotion*, 23(7):1307–1351, 2009.

Schulman, J., Levine, S., Abbeel, P., Jordan, M., and Moritz, P. Trust region policy optimization. In *International conference on machine learning*, pp. 1889–1897. PMLR, 2015.

Schulman, J., Wolski, F., Dhariwal, P., Radford, A., and Klimov, O. Proximal policy optimization algorithms. *arXiv preprint arXiv:1707.06347*, 2017.

Shao, Z., Wang, P., Zhu, Q., Xu, R., Song, J., Bi, X., Zhang, H., Zhang, M., Li, Y., Wu, Y., et al. Deepseekmath: Pushing the limits of mathematical reasoning in open language models. *arXiv preprint arXiv:2402.03300*, 2024.

Sutton, R. S., McAllester, D., Singh, S., and Mansour, Y. Policy gradient methods for reinforcement learning with function approximation. *Advances in neural information processing systems*, 12, 1999.

Team, G., Kamath, A., Ferret, J., Pathak, S., Vieillard, N., Merhej, R., Perrin, S., Matejovicova, T., Ramé, A., Rivière, M., et al. Gemma 3 technical report. *arXiv preprint arXiv:2503.19786*, 2025.

Teh, Y., Bapst, V., Czarnecki, W. M., Quan, J., Kirkpatrick, J., Hadsell, R., Heess, N., and Pascanu, R. Distral: Robust multitask reinforcement learning. *Advances in neural information processing systems*, 30, 2017.

Valstar, M., Gratch, J., Schuller, B., Ringeval, F., Lalanne, D., Torres Torres, M., Scherer, S., Stratou, G., Cowie, R., and Pantic, M. Avec 2016: Depression, mood, and emotion recognition workshop and challenge. In *Proceedings of the 6th International Workshop on Audio/Visual Emotion Challenge*, pp. 3–10. ACM, 2016.

Wilf, A., Mathur, L., Mathew, S., Ko, C., Kebe, Y., Liang, P. P., and Morency, L.-P. Social-iq 2.0 challenge: Benchmarking multimodal social understanding. <https://github.com/abwilf/Social-IQ-2.0-Challenge>, 2023.

Wu, J., Dang, T., Sethu, V., and Ambikairajah, E. A novel markovian framework for integrating absolute and relative ordinal emotion information. *IEEE Transactions on Affective Computing*, 14(3):2089–2101, 2022.

Xu, J., Guo, Z., He, J., Hu, H., He, T., Bai, S., Chen, K., Wang, J., Fan, Y., Dang, K., et al. Qwen2. 5-omni technical report. *arXiv preprint arXiv:2503.20215*, 2025a.

Xu, J., Guo, Z., Hu, H., Chu, Y., Wang, X., He, J., Wang, Y., Shi, X., He, T., Zhu, X., et al. Qwen3-omni technical report. *arXiv preprint arXiv:2509.17765*, 2025b.

Yang, Q., Yao, S., Chen, W., Fu, S., Bai, D., Zhao, J., Sun, B., Yin, B., Wei, X., and Zhou, J. Humanomniv2: From understanding to omni-modal reasoning with context. *arXiv preprint arXiv:2506.21277*, 2025.

Yannakakis, G. N., Cowie, R., and Busso, C. The ordinal nature of emotions: An emerging approach. *IEEE Transactions on Affective Computing*, 12(1):16–35, 2018.

Yu, J. et al. Ch-sims v2: A chinese multimodal sentiment analysis dataset. In *Proceedings of the 30th ACM International Conference on Multimedia*, pp. 1234–1243, 2022.

Yu, Q., Zhang, Z., Zhu, R., Yuan, Y., Zuo, X., Yue, Y., Dai, W., Fan, T., Liu, G., Liu, L., et al. Dapo: An open-source llm reinforcement learning system at scale. *arXiv preprint arXiv:2503.14476*, 2025.

Yu, T., Kumar, S., Gupta, A., Levine, S., Hausman, K., and Finn, C. Gradient surgery for multi-task learning. In *Advances in Neural Information Processing Systems*, volume 33, pp. 5824–5836, 2020.

Zadeh, A., Zellers, R., Pincus, E., and Morency, L.-P. MOSI: Multimodal corpus of sentiment intensity and subjectivity analysis in online opinion videos. *arXiv preprint arXiv:1606.06259*, 2016.

Zadeh, A., Liang, P. P., Poria, S., Cambria, E., and Morency, L.-P. Multimodal language analysis in the wild: CMU-MOSEI dataset and interpretable dynamic fusion graph. In *ACL*, pp. 2236–2246, 2018.

Zhang, J. and Zuo, C. Grpo-lead: A difficulty-aware reinforcement learning approach for concise mathematical reasoning in language models. *arXiv preprint arXiv:2504.09696*, 2025.

Zhang, X. et al. Mental-perceiver: Multimodal mental health dataset and model. In *Proceedings of the AAAI Conference on Artificial Intelligence*, 2025.

## A. HARPO Algorithm Block

We describe the HARPO procedure in Algorithm 1.

---

**Algorithm 1** HARPO Heterogeneity Aware Relative Policy Optimization

---

**Input:** task set  $\mathcal{M}$ ; batch  $\{(m, q)\} \sim \mathcal{D}$ , where  $m \in \mathcal{M}$  indexes tasks and  $q$  denotes a sample from task  $m$ ; rollout groups  $\{G_{(m, q)}\}$  with rewards  $\{r_{(m, q, i)}\}$ ;  $\varepsilon > 0$ ;  $\beta_\rho, \beta_s \in [0, 1]$ ; previous inertial states  $\bar{p}^{(t-1)}$  and  $s^{(t-1)}$

**Output:** updated policy parameters  $\theta$

**Construct group-normalized advantages:**

**for all**  $(m, q)$  in batch **do**

$$\hat{\mu}_{(m, q)} \leftarrow \frac{1}{|G_{(m, q)}|} \sum_{i \in G_{(m, q)}} r_{(m, q, i)}$$

$$\hat{\sigma}_{(m, q)} \leftarrow \sqrt{\frac{1}{|G_{(m, q)}|} \sum_{i \in G_{(m, q)}} (r_{(m, q, i)} - \hat{\mu}_{(m, q)})^2}$$

**for all**  $i \in G_{(m, q)}$  **do**

$$\hat{A}_{(m, q, i)}^{(t)} \leftarrow \frac{r_{(m, q, i)} - \hat{\mu}_{(m, q)}}{\hat{\sigma}_{(m, q)} + \varepsilon}$$

**end for**

**end for**

**Construct contribution signals:**

**for all**  $(m, q)$  in batch **do**

$$p_{(m, q)}^{(t)} \leftarrow \frac{1}{|G_{(m, q)}|} \sum_{i \in G_{(m, q)}} |\hat{A}_{(m, q, i)}^{(t)}|$$

$$\bar{p}_{(m, q)}^{(t)} \leftarrow \beta_\rho \bar{p}_{(m, q)}^{(t-1)} + (1 - \beta_\rho) p_{(m, q)}^{(t)}$$

**end for**

**for all**  $m$  with samples in batch **do**

$$p_m^{(t)} \leftarrow \frac{\sum_{q \in \mathcal{Q}_m^{(t)}} \sum_{i \in G_{(m, q)}} |\hat{A}_{(m, q, i)}^{(t)}|}{\sum_{q \in \mathcal{Q}_m^{(t)}} |G_{(m, q)}|}$$

$$\bar{p}_m^{(t)} \leftarrow \beta_\rho \bar{p}_m^{(t-1)} + (1 - \beta_\rho) p_m^{(t)}$$

**end for**

**Construct geometric references:**

**for all**  $m$  with samples in batch **do**

$$\bar{p}_{\text{ref}, m}^{(t)} \leftarrow \left( \prod_{q \in \mathcal{Q}_m^{(t)}} \bar{p}_{(m, q)}^{(t)} \right)^{1/|\mathcal{Q}_m^{(t)}|}$$

**end for**

$$\bar{p}_{\text{ref}, \mathcal{M}}^{(t)} \leftarrow \left( \prod_{m \in \mathcal{M}} \bar{p}_m^{(t)} \right)^{1/|\mathcal{M}|}$$

**Construct modulation factors:**

**for all**  $(m, q)$  in batch **do**

$$s_{(m, q)} \leftarrow \bar{p}_{\text{ref}, m}^{(t)} / \bar{p}_{(m, q)}^{(t)}$$

$$s_{(m, q)}^{(t)} \leftarrow \left( s_{(m, q)}^{(t-1)} \right)^{\beta_s} (s_{(m, q)})^{1-\beta_s}$$

**end for**

**for all**  $m$  with samples in batch **do**

$$s_m \leftarrow \bar{p}_{\text{ref}, \mathcal{M}}^{(t)} / \bar{p}_m^{(t)}$$

$$s_m^{(t)} \leftarrow \left( s_m^{(t-1)} \right)^{\beta_s} (s_m)^{1-\beta_s}$$

**end for**

**Obtain HARPO-modulated advantages:**

**for all**  $(m, q)$  in batch **do**

**for all**  $i \in G_{(m, q)}$  **do**

$$A_{(m, q, i)}^{H(t)} \leftarrow s_{(m, q)}^{(t)} s_m^{(t)} \hat{A}_{(m, q, i)}^{(t)}$$

**end for**

**end for**

**Optimize policy with HARPO objective:**

Construct PPO-clipped surrogate  $\tilde{A}_{(m, q, i):k}^H(\theta)$  from  $A_{(m, q, i)}^{H(t)}$ , in the same fashion as Eq. (14)

Update  $\theta$  by maximizing  $J_{\text{HARPO}}(\theta)$  using  $\tilde{A}_{(m, q, i):k}^H(\theta)$  (Eq. (12))

---

## B. Additional Details on the Human Behavioral Atlas Benchmark

### B.1. Tasks and Datasets

Human Behavioral Atlas (Ong et al., 2026) comprises approximately 100k samples, with 10 tasks and 13 datasets; we summarize the benchmark below for completeness, with details following the original benchmark description:

The tasks for the benchmark include Sentiment polarity (SEN): classifying attitudes as positive, negative, or neutral; emotion recognition (EMO): identifying emotions (anger, joy, sadness); social reasoning (SOC): understanding socially grounded judgments like empathy or appropriateness; intent recognition (INT): identifying the underlying purpose behind a behavior; and non-verbal communication (NVC): interpreting gestures and facial expressions. They also cover humor detection (HUM), sarcasm detection (SAR), anxiety detection (ANX), depression detection (DEP), and PTSD detection (PTSD).

Each task may be associated with one or more datasets. We summarize the benchmark datasets as follows. CMU-MOSEI (Zadeh et al., 2018) is a large-scale multimodal dataset annotated for sentiment and emotion in real-world opinionated videos. MELD (Poria et al., 2019) provides utterance-level emotion and sentiment annotations from multi-party dialogues in the TV series *Friends*. UR-FUNNYv2 (Hasan et al., 2019) contains multimodal TED talk clips annotated for humor. MUStARD (Castro et al., 2019) is a multimodal sarcasm detection dataset constructed from television show dialogues. DAIC-WOZ (Valstar et al., 2016) consists of multimodal clinical interviews for depression assessment. CREMA-D (Cao et al., 2014) is an acted emotional speech dataset with categorical emotion labels. CH-SIMSv2 (Yu et al., 2022) comprises multimodal sentiment annotations from simulated human–computer interactions. MMPsy (Zhang et al., 2025) is a multimodal mental health dataset annotated for anxiety and depression. PTSD in the Wild (Sawadogo et al., 2024) contains real-world videos annotated for post-traumatic stress disorder. TESS (Pichora-Fuller & Dupuis, 2020) is an emotional speech dataset with acted portrayals of discrete emotions. Social-IQ 2 (Wilf et al., 2023) evaluates social intelligence via reasoning over human interactions in video. IntentQA (Li et al., 2023b) is a video question-answering dataset focused on intent inference in everyday scenarios. MimeQA (Li et al., 2025) evaluates nonverbal social reasoning using gesture-based video question answering.

We report from the original paper, a Tab. 4 which summarizes the datasets associated task, modalities, sample count and evaluation metric. For completeness, the paper also includes the different dimensions of human behavior that each dataset belongs to. These include, *affective states* (Aff), which capture feelings, emotions and sentiments; *cognitive states* (Cog), which reflect internal mental processes such as reasoning or attention inferred from observable behavior; *pathological states* (Path), which correspond to psychological or psychiatric conditions assessed through verbal or nonverbal indicators; and *social processes* (Soc), which characterize social interaction and communicative behaviors such as humor, intent, and cooperation.

Table 4. Datasets and their associated tasks and human behavior dimensions in Human Behavior Atlas. The modalities T, A, V stand for text, audio and vision respectively. The tasks can fall into two categories, CLS = classification (evaluated by direct label matching). TXTR = text-response (evaluated by an LLM judge).

Dataset	Dimension	Task(s)	Task Type	Modalities	Samples	Eval. Metric
CMU-MOSEI	Aff; Cog	EMO, SEN	CLS	T / A / V	31,454	Binary weighted F1 (SEN), Mean weighted acc. (EMO)
MELD	Aff; Soc; Cog	EMO, SEN	CLS	T / A / V	27,412	Binary weighted F1 (SEN), Mean weighted acc. (EMO)
TESS	Aff; Cog	EMO	CLS	T / A / –	2,800	Mean weighted accuracy
CREMA-D	Aff	EMO	CLS	T / A / –	7,442	Mean weighted accuracy
CH-SIMSv2	Aff	SEN	CLS	T / A / V	4,403	Binary weighted F1
Social-IQ 2.0	Soc; Cog	SOC	TXTR	T / A / V	6,437	Accuracy (LLM–Judge)
IntentQA	Soc; Cog	INT	TXTR	T / A / V	16,297	Accuracy (LLM–Judge)
MimeQA	Soc	NVC	TXTR	T / A / V	806	Accuracy (LLM–Judge)
UR-FUNNYv2	Soc	HUM	CLS	T / A / V	2,125	Weighted F1
MUStARD	Soc	SAR	CLS	T / A / V	690	Weighted F1
DAIC-WOZ	Path	DEP	CLS	T / A / –	189	Weighted F1
MMPsy	Path	DEP, ANX	CLS	T / – / –	1,275	Weighted F1
PTSD-in-the-Wild	Path	PTSD	CLS	T / A / V	634	Weighted F1

## B.2. Evaluation Metrics

We follow the same evaluation metrics utilized in Human Behavior Atlas, which specifically account for the task-specific nuances. The summary of the metrics utilized for each task is found in Tab. 4.

For HUM (Humour Detection), SAR (Sarcasm Detection), DEP (Depression Detection), ANX (Anxiety Detection), and PTSD (PTSD Detection), the weighted F1 score is computed:

$$F1 = \frac{2 \cdot \text{Precision} \cdot \text{Recall}}{\text{Precision} + \text{Recall}},$$

where,

$$\text{Precision} = \frac{TP}{TP + FP}, \quad \text{Recall} = \frac{TP}{TP + FN}.$$

The weighted F1 is then computed as:

$$\text{Weighted-F1} = \sum_{c \in C} \frac{n_c}{N} \cdot F1_c,$$

where  $n_c$  is the number of true instances in class  $c$ ,  $N$  is the total number of instances, and  $C$  is the set of classes.

SEN (Sentiment Detection) utilizes binary weighted F1, which applies the same formula but only over the positive and negative sentiment classes, where fine-grained sentiment scales (i.e., weakly positive or weakly negative) are mapped into positive or negative classes respectively. This accounts for the differences in sentiment-scale labelling across the SEN datasets.

For EMO (Emotion Recognition), the mean/ average weighted accuracy across all emotion classes (e.g., fear, surprise, joy) is calculated, using the weighted accuracy formula, following Liang et al. (2018):

$$\text{Weighted-Accuracy} = 0.5 \cdot \frac{TP}{P} + 0.5 \cdot \frac{TN}{N},$$

where  $TP$  and  $TN$  are the number of true positives and true negatives for the target class, and  $P$  and  $N$  denote the total number of positive and negative samples, respectively.

For free-text response QA tasks such as NVC (Non-Verbal Communication), INT (Intent Recognition), and SOC (Social Reasoning), an LLM judge (GPT-5 nano (OpenAI, 2025)) is used to grade the generated responses. Specifically, task-specific prompts are provided to the LLM judge and the proportion of responses marked as TRUE is recorded as an estimate of accuracy:

$$\text{Accuracy} = \frac{\text{number of TRUE responses}}{\text{number of total responses}}$$

The full grading prompts can be found in the original Human Behavior paper (Ong et al., 2026).

## C. Experimental Settings.

### C.1. Hyperparameter Settings

We train all methods for up to 5 epochs with early stopping based on validation performance. Validation is performed every 50 training steps. Early stopping is triggered if the validation metric does not improve for 5 consecutive validation runs (i.e., over 250 training steps). This stopping criterion helps reduce the impact of short-horizon fluctuations in validation metrics that arise from the high variance and non-stationarity of on-policy sampling (Henderson et al., 2018). We select the checkpoint achieving the highest average validation weighted F1 score.

From Tab. 1, model results (i.e., Gemma-3-4B (Team et al., 2025), Qwen 2.5-Omni-7B (Xu et al., 2025a), Qwen 2.5-VL-7B (Bai et al., 2025), OmniSapiens-7B RL (Ong et al., 2026), HumanOmniV2-7B (Yang et al., 2025) are taken from the Human Behavior Atlas benchmark paper (Ong et al., 2026)), while we run the evaluation of Qwen 3-VL-8B Instruct (Xu et al., 2025b) using its implementation on Huggingface<sup>4</sup>.

On the other hand, we implement the reinforcement learning training algorithms in Tab. 1 (i.e., RLOO (Ahmadian et al., 2024), RE++ (Hu, 2025), GPG (Chu et al., 2025), GRPO (Shao et al., 2024)) using the VERL package<sup>5</sup>. To enable fair

<sup>4</sup><https://huggingface.co>

<sup>5</sup><https://github.com/volcengine/verl>

comparison with HARPO, all reinforcement learning methods are run on the same Human Behavior Atlas benchmark, with the same base model, Qwen 2.5-Omni-7B (Xu et al., 2025a), and exactly the same reward design in Sec. 3.3. For the RL baselines, we follow standard practice by reusing the hyperparameter configurations reported in the original papers, thereby preserving the authors’ intended optimization settings. For HARPO, we retain the learning rate used by GRPO ( $1 \times 10^{-6}$ ), since HARPO retains the update structure as GRPO, and we set  $\beta_p, \beta_s$  in the inertial control Eq. (11) as 0.95. We also utilize the AdamW optimizer and omit explicit KL regularization. This is motivated by HARPO’s advantage modulation, which already acts to regularize policy updates, and is aligned with prior literature that strict KL constraints are not always necessary in on-policy training (Yu et al., 2025). For all reinforcement learning methods, we fix the number of rollouts to 5, utilize the same effective batch size of 256 with PPO-mini-batch size of 128, and set the prompt and response lengths to 4096 and 2048 respectively. All methods are run on 4 Nvidia H200s as well as 4 Nvidia RTX PRO 6000 Blackwell GPUs.

## C.2. Full Details on Reward Design

From Sec. 3.3, we utilize a final reward per sample that combines task accuracy  $r_{task}$ , format correctness  $r_{fmt}$ , length penalty  $r_{len}$ . We summarize this below, with format weight  $w_{fmt} = 0.2$  and length scale  $\lambda_{len} = 0.75$ , where  $r_{task}$  can be  $r_{cls}$  or  $r_{qa}$ , depending on if the sample belongs to a classification or QA task respectively:

$$r = (1 - w_{fmt}) r_{task} + w_{fmt} r_{fmt} + \lambda_{len} r_{len},$$

We provide additional details on  $r_{task}, r_{fmt}, r_{len}$ . For  $r_{task}$ , it can either be classification reward  $r_{cls}$ , or question-answering reward  $r_{qa}$ , depending on whether the sample involves a classification response or a free-text answer respectively.  $r_{cls}$  is computed using a binary score for whether the predicted label exactly matches the ground truth label.  $r_{qa}$  leverages a cosine similarity reward that compares the embedding of the predicted free text sequence and the ground truth, leveraging MiniLM-L6-v2<sup>6</sup> as the embedding model. Because cosine similarity typically falls between  $[-1, 1]$ , we ensure that the values are transformed into the range of  $[0, 1]$ , such that it is compatible with reward assignment. We summarise this below, where  $\hat{y}$  is the predicted response (which contains just the answer without reasoning trace) and  $y$  is the ground truth:

$$r_{task}(\hat{y}, y) = \begin{cases} r_{cls}(\hat{y}, y), & \text{if classification,} \\ r_{qa}(\hat{y}, y), & \text{if free-text QA.} \end{cases}$$

$$r_{cls}(\hat{y}, y) = \begin{cases} 1, & \hat{y} = y, \\ 0, & \text{otherwise.} \end{cases}$$

$$r_{qa}(\hat{y}, y) = \frac{\cos(e(\hat{y}), e(y)) + 1}{2}, \quad \cos(u, v) = \frac{u^\top v}{\|u\|_2 \|v\|_2}, \quad u = e(\hat{y}), v = e(y).$$

For the formatting reward  $r_{fmt}$ , we assign a binary reward based on whether the generated response strictly follows the output format specified in the prompt. In particular, we provide the model the following system prompt:

```
{ content }
You FIRST think about the reasoning process as an internal monologue and then
provide the final answer. The reasoning process MUST BE enclosed within <
think> </think> tags. The final answer MUST BE put in \boxed{ }.
```

A response receives  $r_{fmt} = 1$  if and only if it contains `<think>` and `</think>` tags, followed by a final prediction enclosed in `\boxed`, in this order; otherwise,  $r_{fmt} = 0$ . This check is applied to the full response and enforces adherence to the prescribed output schema.

Finally, we provide a overlong length penalty,  $r_{len}$  which follows Zhang & Zuo (2025) to prevent excessive length and verbosity of responses. Accordingly, let  $\ell$  be response length, we use a max  $L_{\max}$  of 812 tokens and buffer length  $B$  of 128

<sup>6</sup><https://huggingface.co/sentence-transformers/all-MiniLM-L6-v2>

tokens. The penalty is:

$$r_{\text{len}}(\ell) = \begin{cases} 0, & \ell \leq L_{\max} - B, \\ \frac{(L_{\max} - B) - \ell}{B}, & L_{\max} - B < \ell \leq L_{\max}, \\ -1, & \ell > L_{\max}. \end{cases}$$

## D. Additional Formulas

### D.1. Full GRPO Formulation

For completeness, we provide the full formulation of GRPO in Sec. 3.1, including the surrogate objective and importance-sampling formulation.

Accordingly, for task  $m$  and sample  $q$ , GRPO samples a rollout group  $G_{(m,q)}$  of responses  $\{o_{(m,q,i)}\}$ , where  $i \in G_{(m,q)}$  indexes individual rollouts (i.e., a sampled response) with rewards  $r_{(m,q,i)}$ , computing the group-normalized advantage:

$$\hat{A}_{(m,q,i)} = \frac{r_{(m,q,i)} - \hat{\mu}_{G_{(m,q)}}}{\hat{\sigma}_{G_{(m,q)}} + \varepsilon}, \quad (13)$$

where  $\hat{\mu}_{G_{(m,q)}}$  and  $\hat{\sigma}_{G_{(m,q)}}$  are the empirical mean and standard deviation of  $\{r_{(m,q,i)}\}_{i=1}^{|G_{(m,q)}|}$ . GRPO then optimizes  $\pi_{\theta}(a | s)$  by performing a PPO-style trust-region update. At token position  $k$  of response  $o_{(m,q,i)}$ ,  $\varphi_{(m,q,i):k}(\theta)$  denotes the importance sampling ratio between  $\pi_{\theta}$  and the old policy  $\pi_{\theta_{\text{old}}}$ ,  $\tilde{A}_{(m,q,i):k}(\theta)$  denotes the PPO-clipped surrogate using  $\hat{A}_{(m,q,i)}$ , and  $J_{\text{GRPO}}(\theta)$  averages this surrogate over tokens and rollout samples with an optional KL penalty to a reference policy  $\pi_{\text{ref}}$  (with weight  $\beta$ ). We summarize these with a compact objective:

$$\begin{aligned} \varphi_{(m,q,i):k}(\theta) &= \frac{\pi_{\theta}(o_{(m,q,i):k} | q, o_{(m,q,i):<k})}{\pi_{\theta_{\text{old}}}(o_{(m,q,i):k} | q, o_{(m,q,i):<k})} \\ \tilde{A}_{(m,q,i):k}(\theta) &= \min\left(\varphi_{(m,q,i):k}(\theta) \hat{A}_{(m,q,i)}, \right. \\ &\quad \left. \text{clip}\left(\varphi_{(m,q,i):k}(\theta), 1 - \epsilon, 1 + \epsilon\right) \hat{A}_{(m,q,i)}\right) \\ J_{\text{GRPO}}(\theta) &= \mathbb{E}_{q \sim \mathcal{D}_m} \mathbb{E}_{\{o_{(m,q,i)}\} \sim \pi_{\theta_{\text{old}}}} \left[ \frac{1}{|G_{(m,q)}|} \sum_{i=1}^{|G_{(m,q)}|} \right. \\ &\quad \left. \frac{1}{n_{o_{(m,q,i)}}} \sum_{k=1}^{n_{o_{(m,q,i)}}} \tilde{A}_{(m,q,i):k}(\theta) \right] - \beta \mathbb{E}[D_{\text{KL}}(\pi_{\theta} \| \pi_{\text{ref}})]. \end{aligned} \quad (14)$$

### D.2. Additional HARPO Details

In Sec. 3.2, we explained the structured modulation utilized by HARPO, which constructs modulation factors by comparing contribution signals to a geometric mean reference. We provide further details on why this construction yields modulation factors whose geometric mean equals 1, ensuring that multiplicative upscaling from certain modulation factors is exactly compensated by downscaling from others.

Fix an iteration  $t$  and a task  $m$ , and let  $\mathcal{Q}_m^{(t)}$  denote the set of samples associated with task  $m$ . The sample-level geometric reference is defined as:

$$\bar{p}_{\text{ref},m}^{(t)} = \left( \prod_{q \in \mathcal{Q}_m^{(t)}} p_{(m,q)}^{(t)} \right)^{\frac{1}{|\mathcal{Q}_m^{(t)}|}}.$$

Using this reference, the sample-level modulation factor for each sample  $q$  is constructed as:

$$s_{(m,q)}^{(t)} = \frac{\bar{p}_{\text{ref},m}^{(t)}}{p_{(m,q)}^{(t)}}.$$

Taking the product over all samples in  $\mathcal{Q}_m^{(t)}$  yields:

$$\prod_{q \in \mathcal{Q}_m^{(t)}} s_{(m,q)}^{(t)} = \prod_{q \in \mathcal{Q}_m^{(t)}} \frac{\bar{p}_{\text{ref},m}^{(t)}}{p_{(m,q)}^{(t)}} = \frac{(\bar{p}_{\text{ref},m}^{(t)})^{|\mathcal{Q}_m^{(t)}|}}{\prod_{q \in \mathcal{Q}_m^{(t)}} p_{(m,q)}^{(t)}}.$$

By definition of the geometric mean:

$$(\bar{p}_{\text{ref},m}^{(t)})^{|\mathcal{Q}_m^{(t)}|} = \prod_{q \in \mathcal{Q}_m^{(t)}} p_{(m,q)}^{(t)},$$

and therefore:

$$\prod_{q \in \mathcal{Q}_m^{(t)}} s_{(m,q)}^{(t)} = 1.$$

This shows that the sample-level modulation factors possess a geometric mean of 1.

An identical argument applies at the task-level. Let  $\mathcal{M}$  denote the set of tasks and define the task-level geometric reference as

$$\bar{p}_{\text{ref},\mathcal{M}}^{(t)} = \left( \prod_{m \in \mathcal{M}} p_m^{(t)} \right)^{\frac{1}{|\mathcal{M}|}}.$$

The task-level modulation factors are given by

$$s_m^{(t)} = \frac{\bar{p}_{\text{ref},\mathcal{M}}^{(t)}}{p_m^{(t)}}.$$

Taking the product over all tasks yields

$$\prod_{m \in \mathcal{M}} s_m^{(t)} = 1.$$

Therefore, the modulation factors possess a geometric mean of 1 at both the sample and task-levels, ensuring that multiplicative upscaling from some modulation factors is exactly compensated by downscaling from others. Hence, the factors cannot simultaneously enlarge or shrink all advantages at the sample or task-level, mitigating unintended influence on the effective global step size.

## E. Additional Results

### E.1. Full Ablation Results

We provide the per task and per dataset breakdown of the results from the ablation in the following. Tab. 5 represents the task-level performance of the ablations, whereas Tab. 6 represents the per-dataset performance breakdown of all ablations.

Table 5. Per-task performance (%) for HARPO ablations across behavioral tasks. Each value is the arithmetic mean over datasets associated with the task. Avg. Rank is computed across tasks using per-task ranks (higher is better; ties use average rank), and then averaged over tasks (lower is better). Rows with missing task values are omitted from ranking.

Variant	EMO	HUM	INT	PTSD	ANX	DEP	SEN	SAR	SOC	NVC	Avg. Rank ↓
<b>HARPO</b>	76.55	<b>69.85</b>	50.52	<b>98.39</b>	<b>91.98</b>	<b>78.87</b>	<b>77.61</b>	70.64	25.40	14.54	<b>1.90</b>
w/o structured modulation	<b>78.44</b>	66.61	50.38	<b>98.39</b>	90.68	77.01	77.48	<b>72.68</b>	29.08	<b>15.12</b>	2.00
w/o inertial control	76.42	63.05	<b>53.28</b>	<b>98.39</b>	90.68	76.48	71.92	62.68	<b>30.12</b>	13.95	2.70
w/o sample-level modulation	77.27	67.82	50.94	<b>98.39</b>	90.68	71.04	76.37	68.19	<b>29.43</b>	12.21	2.60

Table 6. Ablation results for HARPO components, grouped by behavioral tasks and datasets. Following the unified metrics proposed in the Human Behavior Atlas Benchmark (Ong et al., 2026), we use binary weighted F1 for SEN; mean per-class weighted accuracy for EMO; weighted F1 for HUM, SAR, ANX, DEP, PTSD; and LLM-Judge accuracy for SOC, INT, NVC.

Model / Ablations	EMO				HUM				INT				PTSD				ANX				DEP				SEN				SAR				SOC				NVC			
	CREMA-D	MELD (E)	MOSEI (E)	TESS	UR-FUNNY	IntentQA	PTSD-WILD	MMPSY (A)	MMPSY (D)	DAIC-WOZ	MELD (S)	CH-SIMSV2	MOSEI (S)	MUSTARD	Social-IQ 2.0	MineQA																								
<b>HARPO</b>	85.80	69.14	55.45	95.83	69.85	50.52	98.39	91.98	84.53	73.20	75.49	88.71	68.64	70.64	25.40	14.54																								
w/o structured modulation	84.48	71.70	60.36	97.22	66.61	50.38	98.39	90.68	83.20	70.82	70.43	88.37	73.65	72.68	29.08	15.12																								
w/o inertial control	86.49	67.86	56.61	94.72	63.05	53.28	98.39	90.68	82.04	70.92	73.80	84.65	57.32	62.68	30.12	13.95																								
w/o sample-level modulation	84.71	68.92	57.38	98.06	67.82	50.94	98.39	90.68	73.44	68.64	71.61	87.76	69.74	68.19	29.43	12.21																								

### E.2. Full Dataset Results

For brevity, Tab. 1 shows the performance at the task-level. We additionally provide the dataset-level breakdown of these results in the following Tab. 7. We also provided the full dataset breakdown for HARPO and its ablations in Tab. 6.

### E.3. Additional Training Plots

We provide additional training plots to empirically illustrate the training dynamics in our experiments.

We include a Fig. 7 that depicts the advantage distributions of the different behavioral tasks in the Human Behavior Atlas benchmark (Ong et al., 2026). In particular, the right column of Fig. 7 depicts the group-normalized advantages of the tasks SEN, NVC, INT under a GRPO run. The different advantage distributions observed highlights how the behavioral tasks can systematically induce different advantages, as mentioned in Sec. 3.1.

In the left column of this Fig. 7, we compare the advantage distributions with and without sample-level modulation for other tasks (SOC, HUM, NVC). Accordingly, we observe that with sample-level modulation in the HARPO method, the advantage distributions tend to become narrower than without. This coincides with more consistent performance across tasks in Tab. 3 with HARPO achieving an average task rank of 1.90 compared to without sample-level modulation at 2.60.

We include a Fig. 6 to illustrate the task-level modulation factors over time between the ablation that utilizes  $s^{(t)} = 1/p^{(t)}$  and HARPO. To this end, we observe that in the left column of this figure, the geometric mean of the modulation factors are consistently above 2.5. This further illustrates how the modulation factors can induce unintended scaling of the global step size, without geometric centering.

In the same Fig. 6, in the right column, we also observe how the contribution signals  $p^{(t)}$  varies with training for different tasks, SAR, INT, EMO, SOC. Accordingly, we observe that for certain tasks, the task-level contribution signals  $p_m^{(t)}$  can differ by orders of magnitude. For example, the  $p_m^{(t)}$  for INT may exceed EMO by a factor of up to 7. Since these signals are used to construct the modulation factors, the empirical illustrations provide additional context for the considerable variation in modulation factors. This motivates the use of a geometric reference as a practical tool to temper excessively large differences in modulation factors.

Table 7. Full results grouped by behavioral tasks (headers) and their relevant datasets (sub-headers). Following the unified metrics proposed in the Human Behavior Atlas Benchmark (Ong et al., 2026), we use binary weighted F1 for SEN; mean per-class weighted accuracy for EMO; weighted F1 for HUM, SAR, ANX, DEP, PTSD; and LLM-Judge accuracy for SOC, INT, NVC.

Model / Algorithm	EMO			HUM			INT			PTSD			ANX			DEP			SEN			SAR			SOC		NVC	
	CREMA-D	MELD (E)	MOSEI (E)	TESS	UR-FUNNY	IntentQA	PTSD-WILD	MMPSY (A)	MMPSY (D)	DAIC-WOZ	MELD (S)	CH-SIMSV2	MOSEI (S)	MUSTARD	Social-IQ 2.0	MimeQA												
<b>Models</b>																												
Gemma-3-4B	49.50	64.20	56.50	49.90	59.70	22.70	49.90	60.10	78.80	13.70	78.50	81.30	61.70	52.90	19.10	2.30												
Qwen 2.5-Omni-7B	52.10	66.10	58.00	56.80	54.30	25.40	76.00	79.30	79.10	63.60	70.00	71.40	60.20	65.60	25.40	6.90												
Qwen-2.5-VL-7B	50.10	57.10	59.20	49.90	58.30	24.90	75.50	63.10	65.30	62.30	67.40	52.40	31.70	51.10	23.10	9.80												
Qwen 3-VL-8B-Instruct	50.20	70.87	59.44	50.14	66.76	38.00	92.70	42.29	36.38	66.86	68.97	77.19	62.93	63.67	24.94	13.95												
OMNISAPIENS-7B RL	50.10	69.90	58.10	51.00	63.90	48.60	96.80	91.90	81.40	72.90	57.10	39.30	22.40	64.70	30.40	13.30												
HumanOmniV2-7B	56.00	63.30	55.80	63.70	63.80	26.30	82.40	52.70	67.20	63.60	76.80	82.50	63.30	39.50	28.20	9.30												
<b>OMNISAPIENS-7B 2.0 (ours)</b>	<b>85.80</b>	<b>69.14</b>	<b>55.45</b>	<b>95.83</b>	<b>69.85</b>	<b>50.52</b>	<b>98.39</b>	<b>91.98</b>	<b>84.53</b>	<b>73.20</b>	<b>75.49</b>	<b>88.71</b>	<b>68.64</b>	<b>70.64</b>	<b>25.40</b>	<b>14.54</b>												
<b>Training Algorithms</b>																												
RLOO	85.77	67.74	50.05	98.75	67.86	51.73	98.39	90.68	84.26	70.88	67.72	89.64	73.21	62.58	29.54	16.28												
RE++	82.56	66.52	59.05	95.56	60.26	5.01	98.39	93.11	79.09	68.64	66.67	87.86	15.03	50.21	12.64	4.07												
GPG	82.62	69.36	60.00	98.75	69.28	54.21	98.39	90.36	85.88	70.92	75.10	87.77	64.43	45.96	27.93	12.79												
GRPO	82.88	69.85	57.22	95.83	27.56	49.90	98.39	90.42	84.35	70.92	76.28	84.57	71.68	53.58	23.30	11.00												
<b>HARPO (ours)</b>	<b>85.80</b>	<b>69.14</b>	<b>55.45</b>	<b>95.83</b>	<b>69.85</b>	<b>50.52</b>	<b>98.39</b>	<b>91.98</b>	<b>84.53</b>	<b>73.20</b>	<b>75.49</b>	<b>88.71</b>	<b>68.64</b>	<b>70.64</b>	<b>25.40</b>	<b>14.54</b>												

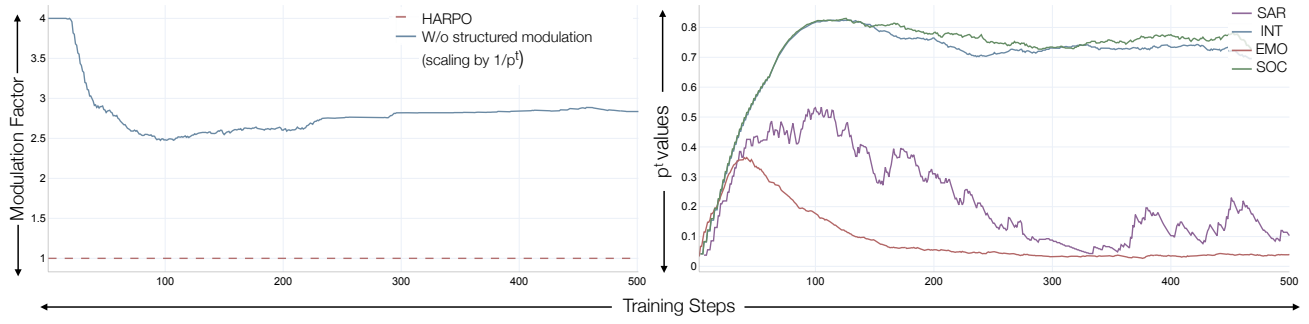


Figure 6. Left: Comparison of geometric mean of the task-level modulation factors  $s_m^{(t)}$  between HARPO and the w/o structured modulation ablation that utilizes  $s^{(t)} = 1/p^{(t)}$ . We observe that the modulation geometric mean of the modulation factors are above 2.5 throughout training. Right: Values of  $p_m^{(t)}$  over training for different tasks SAR, INT, EMO, SOC. We observe that between specific tasks (i.e., INT vs EMO), the task-level contribution signals  $p_m^{(t)}$  can vary by considerable orders of magnitude throughout training.

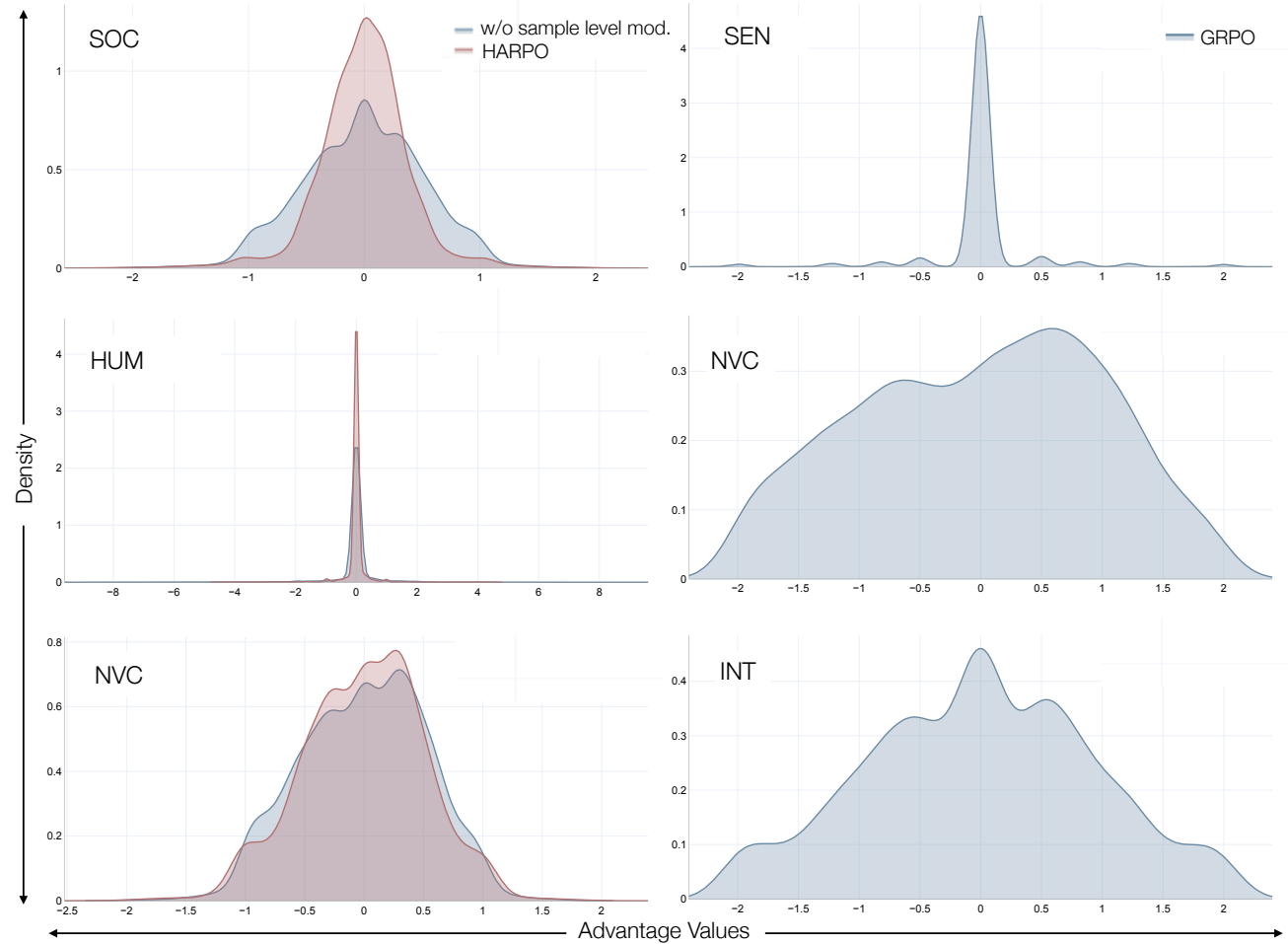


Figure 7. Left: Advantage distributions for HARPO (red) and the ablation (blue) which does not involve sample-level modulation, across the different tasks SOC, HUM, NVC. We observe that HARPO, with sample-level modulation induces a narrower advantage distribution. Right: More plots to depict the group-normalized advantage distributions of different tasks, SEN, NVC, INT. We observe that the different behavioral tasks provide different advantage distributions.